Hindawi
Journal of Nanomaterials
Volume 2018, Article ID 2156895, 7 pages
https://doi.org/10.1155/2018/2156895

*Research Article*

# Low Power Switching Characteristics of CNT Field Effect Transistor Device with Al-Doped $ZrHfO_2$ Gate Dielectric

**Seyoung Oh,[1] Seung Won Lee,[2] Dongjun Kim,[1] Jeong-Hun Choi,[2] Hong-Chul Chae,[3] Sung Mook Choi,[4] Ji-Hoon Ahn,[2] and Byungjin Cho[1]**

[1]*Department of Advanced Material Engineering, Chungbuk National University, Chungbuk 28644, Republic of Korea*
[2]*Department of Electronic Material Engineering, Korea Maritime and Ocean University, Busan 49112, Republic of Korea*
[3]*Center for Research Instruments and Experimental Facilities, Chungbuk National University, Chungbuk 28644, Republic of Korea*
[4]*Surface Technology Division, Korea Institute of Materials Science (KIMS), Gyeongnam 51508, Republic of Korea*

Correspondence should be addressed to Ji-Hoon Ahn; ajh1820@kmou.ac.kr and Byungjin Cho; bjcho6885@gmail.com

Received 1 June 2018; Accepted 28 August 2018; Published 8 October 2018

Academic Editor: Miguel A. Correa-Duarte



In this report, we demonstrated a reliable switching effect of carbon nanotube (CNT) field-effect transistor (FET) devices integrated with 99% semiconducting CNT as a channel and high-k oxide as the dielectric. CNT FET devices with high-k oxides of Al-$ZrHfO_2$ and $Al_2O_3$ were electrically characterized and compared. There was no considerable hysteresis in the $Al_2O_3$-based CNT FET device. The Al-$ZrHfO_2$ with a tetragonal phase-based high dielectric constant (~47), designed by an atomic layer deposition process, showed a reliable switching effect as well as low operation voltage (<±3 V). Charge trapping/detrapping process via oxygen vacancy-related defects of Al-$ZrHfO_2$ was proposed as a primary mechanism to explain a current change of a counterclockwise direction and threshold voltage ($V_{th}$) shift for transfer properties. The suggested charge trapping model within bulk oxide was experimentally proven since the hysteresis from the adsorption/desorption of gas molecules to CNT surface was negligible. Endurance characteristics of the CNT switching devices remained stable without any serious current fluctuation during a repetitive cycling test. The memory device with reliable switching properties as well as low operation power would pave a road toward next-generation memory components of portable electronic gadgets.

## 1. Introduction

Carbon nanotube (CNT) has been considered as a promising building block for next-generation electronics such as electronic transistor and sensor since they possess extraordinary physical properties [1–4]. The unique structure of CNT, consisting of strong sigma bonding from sp2 hybrid orbital and pi bonding from unshared electrons, have accelerated the relevant researches. Owing to the nanoscale diameter and large carrier mobility in CNT, the CNT-based electronic memory devices have achieved ultimate integration, high switching ratio, fast switching speed, low power consumption, and nonvolatile information storage capability [5–7]. Particularly, CNT memory device has been implemented by few strategies: electrochemical reaction, floating gating type charge storage element, ferroelectrics, and nanocrystals [5, 6, 8–10].

Meanwhile, the abrupt size reduction of dynamic random-access memory (DRAM) cell keeps pushing on the development of new high-k dielectric materials. Zr- and Hf-based oxides have been applied as a representative dielectric component of complementary metal oxide semiconductor circuit [11]. Furthermore, a $ZrO_2$ film with an ultrathin $Al_2O_3$ layer, deposited by atomic layer deposition (ALD), has been also used in current DRAM capacitor [11]. Diverse crystal structures (monoclinic, cubic, tetragonal, or orthorhombic) of the high-k oxides exist depending on film preparation method, which indicates that the corresponding ALD deposition methods require precise control of precursors, temperature, phase, stoichiometry, and so on. Tetragonal

phase in $ZrO_2$ and $HfO_2$ showed the highest dielectric constant among a few crystal structures aforementioned. However, it is not easy to achieve the tetragonal phase with high dielectric constant since the monoclinic phase is most thermodynamically stable at ambient. Alternatively, doping strategy to stabilize the tetragonal $ZrO_2$ or $HfO_2$ has been concentrated on the development of high dielectric constant oxide materials [11, 12].

Thus, it is so critical to carefully design and integrate material component for implementing ultimately low-powered electronic devices. Furthermore, integration of CNT nanomaterials and high-k dielectric materials with intrinsically electronic trap states is highly required to realize low-powered switching devices, which has rarely been studied. In this work, a reliable switching effect was demonstrated in the CNT field-effect transistor (FET) device which is fabricated by synergistically integrating CNT network channel and Al-doped $ZrHfO_2$ (Al-$ZrHfO_2$) high-k dielectric. The novel Al-$ZrHfO_2$ with a tetragonal phase-based high dielectric constant (~47), deposited by ALD method, allowed a reliable switching effect as well as low operation voltage ($<\pm 3$ V) while there was no switching effect on $Al_2O_3$-based CNT FET device as control device. It was proposed that charge trapping/detrapping process via oxygen vacancy-related defects of Al-$ZrHfO_2$ induced modulation of CNT carrier concentration, leading to current change and threshold voltage ($V_{th}$) shift. The suggested charge trapping model within bulk oxide was theoretically and experimentally validated since the hysteresis from the adsorption/desorption of gas molecules to CNT surface was negligible. The CNT transistor devices would be potential applications for next-generation nonvolatile memory components of portable electronic gadgets.

## 2. Materials and Experimental Method

*2.1. Deposition of High-k Dielectrics.* High-k dielectrics of $Al_2O_3$ and Al-$ZrHfO_2$ thin films were deposited on heavily doped p-type Si substrate (p+ Si, resistivity $< 0.005\ \Omega$·cm) using plasma-enhanced atomic layer deposition (PEALD) with a 6-inch ALD reactor system (iOV d150, iSAC Research). Deposition process of the $Al_2O_3$ thin film was conducted at 300°C using trimethylaluminum (TMA) and $O_2$ plasma with a power of 200 W while the Al-$ZrHfO_2$ thin film was deposited at 280°C using the mixture precursor of tetrakis(ethylmethylamino)zirconium (TEMAZr) and tetrakis(ethylmethylamino)hafnium (TEMAHf) with a molar ratio of 40 : 60 and TMA with $O_2$ plasma as an oxidant. A modified supercycle, consisting of 10 subcycles of $ZrHfO_2$ and one subcycle of Al-$ZrHfO_2$, was applied for uniformly incorporating small amounts of Al dopant into $ZrHfO_2$. As shown in Figure S1a in Supporting Information, $ZrHfO_2$ subcycle is composed of 4 steps: (1) TEMA-ZrHf mixture precursor feeding, (2) Ar purging, (3) $O_2$ plasma, and (4) Ar purging. Al-$ZrHfO_2$ subcycle consists of 6 steps: (1) ZrHf mixture precursor feeding, (2) Ar purging, (3) TMA precursor feeding, (4) Ar purging, (5) $O_2$ plasma, and (6) Ar purging. The resulting amount of Al dopant in the films was analyzed to be ~2.4 at % using X-ray photoelectron spectroscopy. The Al-$ZrHfO_2$ thin films showed an obvious tetragonal phase from X-ray diffraction (Figure S1b in Supporting Information) which features high dielectric constant with high temperature stability. The thickness of $Al_2O_3$ and Al-$ZrHfO_2$ was the same as 30 nm, which was confirmed by ellipsometry measurement.

*2.2. Fabrication Process of CNT Devices.* Ozone treatment was performed on the ALD-deposited high-k oxide ($Al_2O_3$ or Al-$ZrHfO_2$)/p+ Si substrate to form hydroxyl group for (3-aminopropyl)triethoxysilane (APTES) self-assembly monolayer (SAM) treatment. The substrate was dipped into APTES solution dissolved in isopropyl alcohol (IPA) solvent. The APTES SAM, chemically bonded on hydroxyl groups of high-k oxide surface, enabled the formation of dense CNT network by spin-coating method. Next, to eliminate APTES residue, the APTES-functionalized substrate was rinsed by IPA solvent and then sonicated for 5 sec. 99% semiconducting CNT solution (NanoIntegris Inc. concentration: 1 mg/100 mL, mean diameter: 1.4 nm, mean length: 1 $\mu$m, and purification: density gradient ultracentrifugation) was spin-coated onto $Al_2O_3$ or Al-$ZrHfO_2$ high-k dielectric layers/p+ Si substrate. CNT density was optimized by manipulating the number of spin-coating, and 13 times (200 $\mu$L droplet per one time) spin-coating process was done for our CNT devices. The CNT spin-coating consists of a two-step process: acceleration with 500 rpm for 3 sec and duration with 2000 rpm for 30 sec. After CNT coating each, isopropyl alcohol (IPA) was dropped to remove the surfactants in CNT solution and make uniform CNT dispersion. For patterning CNT channel region, photoresist (AZ GXR 601) was spin-coated on predeposited CNT network and then was patterned by photolithography process. The CNT channel was defined with a length of 50 $\mu$m and a width of 500 $\mu$m. After that, the CNT network was etched by ultraviolet-ozone treatment for 10 min. Finally, 50 nm thick Al source-drain electrode patterns were formed by using a thermal evaporator and a shadow mask.

*2.3. Electrical Measurement.* Electrical properties of CNT FET device were measured at ambient condition by utilizing a Keithley 2636B source meter system with the customized measurement software. In the case of vacuum condition measurement, the CNT FET devices were loaded onto the vacuum probe station and then evacuated to ~10 mT by a rotary pump.

## 3. Result and Discussion

To explore the electrical property of devices integrated with high-k dielectric materials and 99% semiconducting CNT channel, three-terminal FET device with back gate structure was fabricated and then electrically tested. Figure 1(a) illustrates a 3D device scheme of the CNT transistor with high-k dielectric/p+ Si substrate. Figure 1(b) shows an optical microscope image of CNT channel region (50 $\mu$m channel length and 500 $\mu$m channel width) which is connected to Al source/drain electrodes. As shown in Figure 1(c), CNT network image, mixed with CNT bundles and single-wall CNTs,

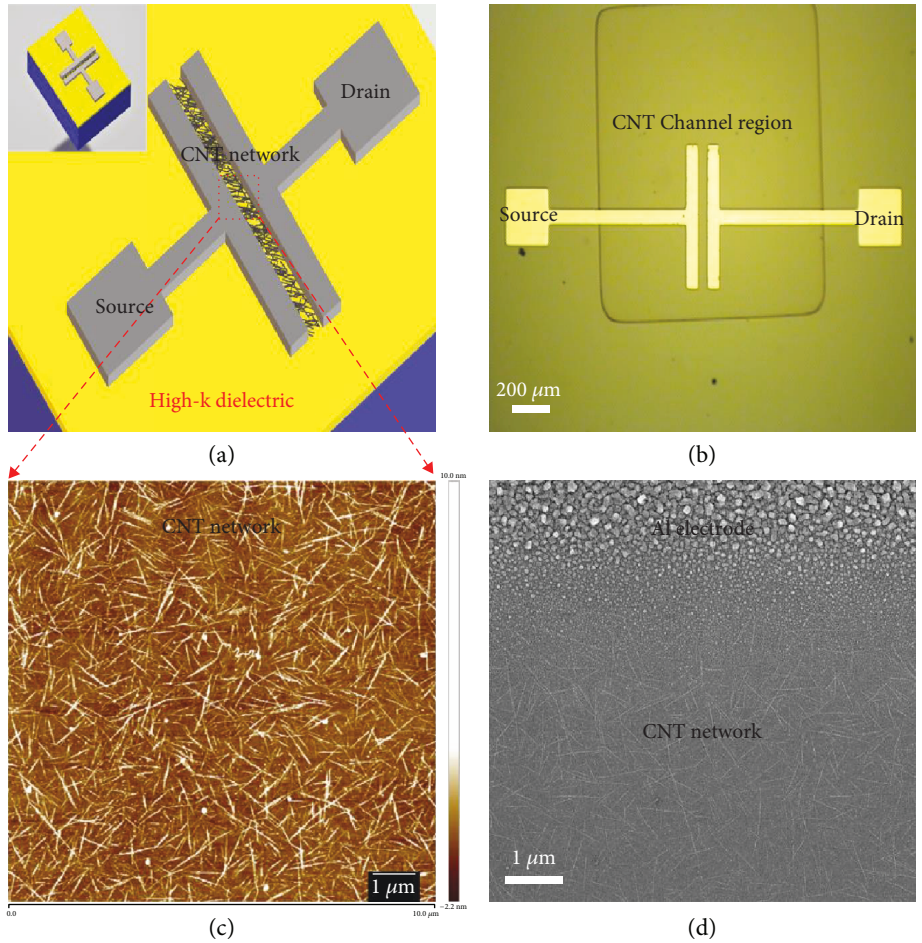


Figure 1: (a) A 3D scheme of CNT FET device on high-k dielectric. (b) An optical microscope image of CNT FET device including source-drain electrode and CNT channel region. (c) An AFM image of CNT network. (d) A SEM image of the interface between CNT network and Al electrode.

was obtained by the scanning process of atomic force microscopy (AFM). The spin-coated bundle CNT network was uniformly dispersed on high-k-deposited Si substrate. The density of our CNT network was optimized by controlling the number of spin-coating, which is able to reproducibly form a uniform CNT network on the chip scale. Fully connected CNT channel was made above the percolation threshold. Interestingly, we observed that the increase in spin-coating times induces a formation of more bundle CNTs, which is attributed to the van der Waals interaction between single-wall CNTs [13]. To observe the physical contact between Al electrode and CNT network, scanning electron microscopy (SEM) image of the Al-CNT interface was obtained as shown in Figure 1(d). Granular Al film was formed on the CNT network, which might be due to the large difference in surface tension of two materials (the surface tension of Al and CNT is 955 and 45.3 mN/m, respectively) [14, 15]. Surface energy of CNT is so low that it is hard to make strong chemical bonding with contact metals. Instead, nucleation and grain growth process of Al would start on energetically active CNT edge sites and then grains merge, forming continuous Al film.

In order to validate the chemical fingerprint of the CNT, we performed auger electron spectroscopy (AES) analysis. Figure 2(a) shows AES spectrum of CNT network film. There were three prominent peaks corresponding to C from CNT network, and Si and O from $SiO_2$ substrate. The kinetic energy of the Si and O peaks was measured to be 1611 and 502 eV. The peak of 275 eV indicates C from CNT, which is consistent with the previous result [16]. AES element mapping image, corresponding to the C peak, was also achieved, showing fully connected CNT bundle tubes on the scanning region (Figure 2(b)). However, we did not observe single-wall CNTs due to the resolution limit of AES analysis.

Electrical properties of CNT FET devices with two different dielectric layers (Al-$ZrHfO_2$ and $Al_2O_3$) were tested and compared. Figure 3(a) shows transfer curves ($I_{DS} - V_{BG}$) of the CNT FET devices measured at fixed $V_{DS}$ of −1 V. $V_{DS}$-$I_{DS}$ of the CNT FET devices under no gating ($V_{BG}$ of 0 V) were also checked, showing different current level to some extent (Figure S2 in Supporting Information). It might be attributed to the deviation in CNT adsorption probability caused by different physical surface properties between $Al_2O_3$ and Al-$ZrHfO_2$. All of two devices were turned on

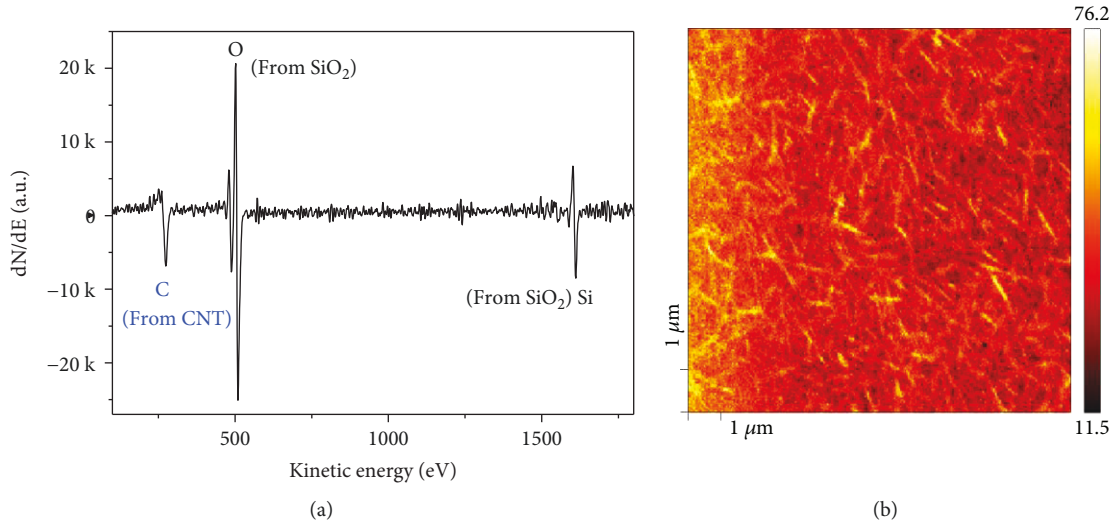


Figure 2: (a) AES spectra of the CNT network film on $Si/SiO_2$. (b) AES-mapping image.

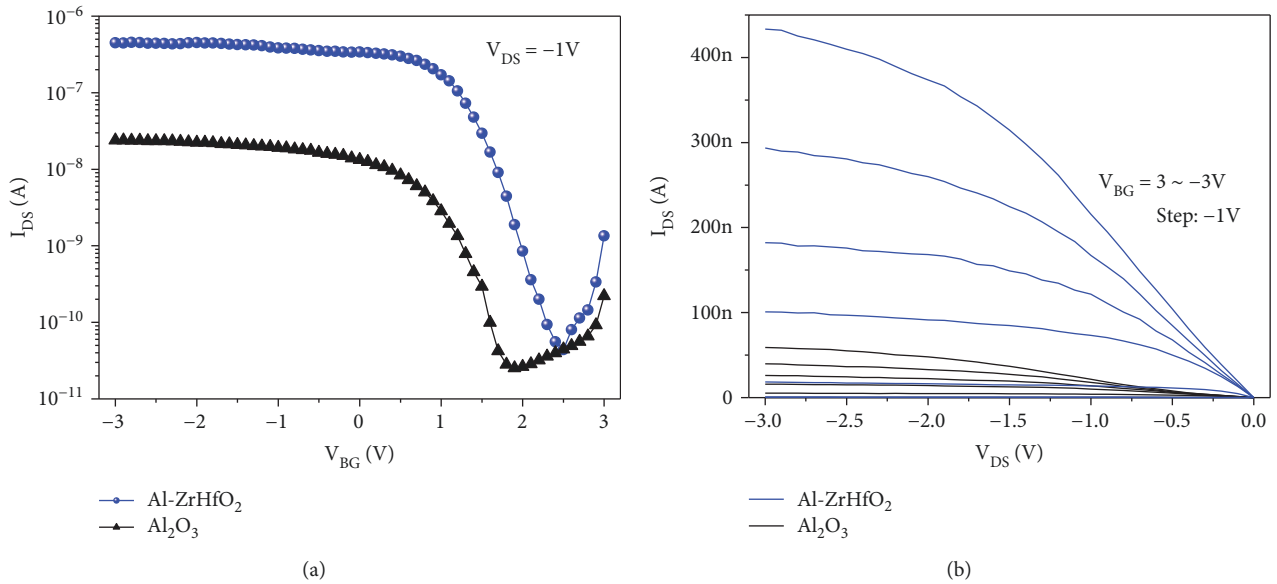


Figure 3: Comparison of (a) transfer characteristics ($V_{BG}$-$I_{DS}$) under $V_{DS} = -1$ V and (b) output characteristics ($V_{DS}$-$I_{DS}$) under $V_{BG} = 3 \sim -3$ V for Al-$ZrHfO_2$ and $Al_2O_3$ CNT FET devices.

during $V_{BG}$ sweeping to reverse direction (3 V to −3 V, step: −0.1 V), which indicates that the CNT possess a p-type semiconducting property with holes as the major carriers. $I_{on}$ and $I_{off}$ of Al-$ZrHfO_2$ CNT FET were $4.5 \times 10^{-7}$ and $4.4 \times 10^{-11}$ A, respectively. Meanwhile, in the case of $Al_2O_3$ CNT FET, the performance was relatively poor since $I_{on}$ and $I_{off}$ were measured to be $\sim 3.2 \times 10^{-8}$ and $1.5 \times 10^{-11}$ A, respectively. Thus, on/off ratio of the Al-$ZrHfO_2$ device ($\sim 10^4$) was five times higher than that of the $Al_2O_3$ device ($\sim 2 \times 10^3$). The threshold voltages ($V_{th}$) of Al-$ZrHfO_2$ and $Al_2O_3$ FET devices were extracted to be 1.6 and 0.1 V, respectively (Figure S3 in Supporting Information). The subthreshold swing was 0.31 V/dec for Al-$ZrHfO_2$ and 0.68 V/dec for the $Al_2O_3$ device. Values of transconductance were 0.29 and 0.01 $\mu$S for Al-$ZrHfO_2$ and $Al_2O_3$ FET. Subthreshold swing of Al-$ZrHfO_2$ CNT FET (310 mV/dec) was approximately two times smaller than that of $Al_2O_3$ CNT FET (680 mV/dec). As shown in Figure 3(b), output characteristics ($I_{DS}$-$V_{DS}$) of two high-k FET devices were measured under variable $V_{BG}$ (3 to −3 V, step: −1 V). Output current increased by 433 nA for Al-$ZrHfO_2$ FET device while $Al_2O_3$ FET device increased by 59 nA. Comparison of essential FET parameters for two devices was also shown in Table S1 in Supporting Information. Indeed, the performance of the Al-$ZrHfO_2$ CNT FET devices was considerably enhanced due to high gating ability to effectively accumulate hole carriers on CNT surface. Particularly, precisely controlled and optimized stoichiometry in Al-$ZrHfO_2$ ternary composition caused a tetragonal phase generating a high dielectric constant. The dielectric constant of Al-$ZrHfO_2$ thin film was increased by an appropriate amount of Al doping. In fact, the dielectric

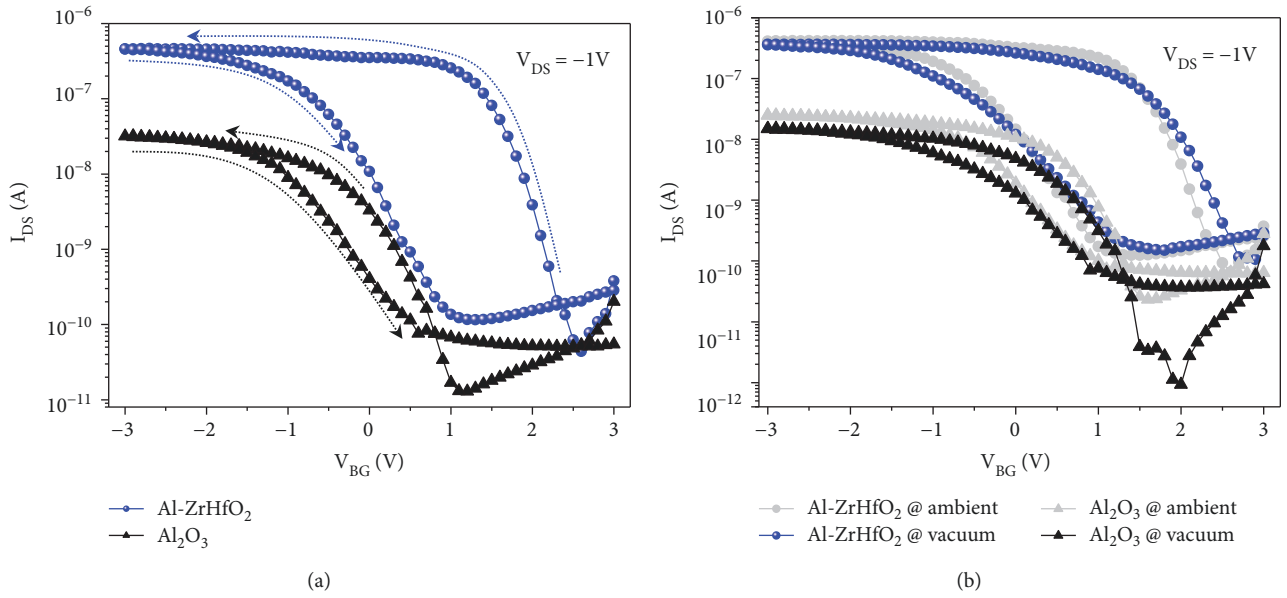


Figure 4: (a) Hysteresis properties of CNT FET devices with Al-ZrHfO$_2$ and Al$_2$O$_3$ high-k. The arrows indicate the directions of $I_{DS}$. (b) Change in hysteresis loop characteristics in ambient and vacuum (~10 mT) condition for each device.

constant of Al-ZrHfO$_2$ thin film used in this experiment was about 47 while that of Al-undoped ZrHfO$_2$ film was only 26. However, the operation of CNT transistor with 100 nm thick SiO$_2$ dielectric (control device) needed a relatively large gating voltage from 30 to −30 V (Figure S4 in Supporting Information).

In order to check memory effect of the high-k CNT FET devices, hysteresis properties of Al-ZrHfO$_2$ and Al$_2$O$_3$ high-k CNT FET devices were tested at ambient condition as shown in Figure 4(a). When $V_{BG}$ swept from 3 to −3 V and returned to 3 V for Al-ZrHfO$_2$ device, the corresponding $V_{th}$ shifted from 1.6 to −0.2 V (memory window of 1.8 V) and $I_{DS}$ showed counterclockwise direction ($I_{DS}$ increase in positive $V_{BG}$ and $I_{DS}$ decrease in negative $V_{BG}$). That is, the double sweeping process to positive $V_{BG}$ ($0 \rightarrow 3 \rightarrow 0$ V) accumulates hole carriers while negative $V_{BG}$ ($0 \rightarrow -3 \rightarrow 0$ V) depletes hole carriers. However, no considerable hysteresis loop was not observed in the Al$_2$O$_3$ device. There are two acceptable models to describe the origin of the oxide-switching phenomena: ferroelectricity and defect-related charge trapping of oxide dielectric. It was previously reported that ferroelectricity in the ZrO$_2$-HfO$_2$ binary oxide system with orthorhombic phase induced the hysteresis loop [17]. However, the phase of our Al-ZrHfO$_2$ ternary system was only tetragonal phase (see Figure S1b in Supporting Information). Undoped ZrHfO$_2$ film exhibits ferroelectricity behavior on polarization-electric curve test while hysteresis characteristic disappears on the Al-doped ZrHfO$_2$ film, indicating typical dielectric polarization behavior. Thus, we can exclude the first model that the ferroelectric properties of Al-ZrHfO$_2$ could induce the switching effect. The most likely explanation can come from the second model where charge traps within the Al-ZrHfO$_2$ govern the hysteresis [7]. Lots of relevant researches have been focused on the study of the charge trapping in HfO$_2$ [18, 19]. Charging and

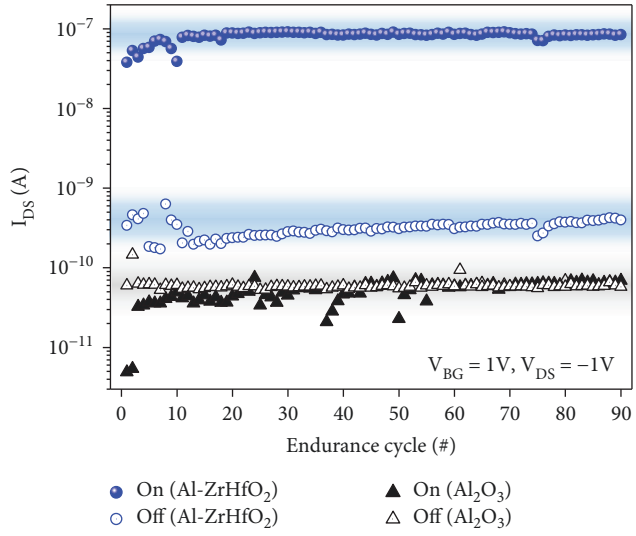


Figure 5: Memory endurance properties of Al-ZrHfO$_2$ and Al$_2$O$_3$ CNT devices during 90 cycling test. On/off current was read at $V_{BG} = 1$ V and $V_{DS} = -1$ V.

discharging occurs via defect-related electronic states in the band gap of Al-ZrHfO$_2$. The defect states available can function as electron traps [7, 20]. These defect states are attributed to oxygen vacancies with a large electron affinity [20–22]. It is highly likely to make more oxygen vacancies in the complex ternary oxide system (Al-ZrHfO$_2$) than simple single component oxide (Al$_2$O$_3$). Based on the trapping model, an applied positive gate voltage fills electrons in defect sites, giving rise to accumulation of major hole carriers in CNT channel due to Coulomb interaction ($I_{DS}$ increase and right shift of $V_{th}$). Meanwhile, a negative gate voltage releases electrons trapped in defect sites, leading to the depletion of hole carriers in CNT ($I_{DS}$

decrease and left shift of $V_{th}$). However, it was expected that the hysteresis properties in nanomaterials with large surface area could be often induced by adsorption and desorption process of ambient gas molecules (oxygen and moisture) on CNT network [23]. In order to confirm the influence of gas molecules on CNT electrical properties, we compared transistor hysteresis characteristics under different testing environment (ambient and vacuum). Figure 4(b) shows a discrepancy of hysteresis loop measured in ambient and vacuum for two high-k FET devices. A remarkable deviation in the hysteresis loop was not found for all of two devices, indicating that influences of gas molecule adsorption on carrier modulation of CNT channel is negligible. Thus, ambient gas molecules affected a little to the hysteresis loop of Al-$ZrHfO_2$ transistor memory devices. Thus, it is strongly acceptable again that such a hysteresis comes from oxygen vacancy-related defects of Al-$ZrHfO_2$ dielectric layer.

As shown in Figure 5, memory endurance was investigated by repetitive 90 sweep cycling test. On and off currents were read at $V_{BG} = 1$ V and $V_{DS} = -1$ V. Electrical properties of two devices remained stable during cycling test. However, Al-$ZrHfO_2$ CNT FET device showed reliable switching characteristics with on/off ratio of ~$10^3$. $Al_2O_3$ FET device did not have a distinct on/off state gap. Thus, Al-$ZrHfO_2$ transistor will be utilized for low-powered nonvolatile memory applications necessary for next-generation portable electronic gadgets.

## 4. Conclusions

We demonstrated the CNT FET device integrated with 99% semiconducting channel and high-k dielectric (Al-$ZrHfO_2$ and $Al_2O_3$), enabling low operation voltage of 3 V. Particularly, tetragonal Al-$ZrHfO_2$ high-k dielectric, deposited by ALD, gave rise to effective gating modulation and switching effect. Proposed model to explain the switching was charge trapping/detrapping process via oxygen vacancy-related defects of Al-$ZrHfO_2$, which is theoretically and experimentally confirmed. Endurance property of the CNT memory devices remained stable without any serious current fluctuation during 90 cycling test. The high-k-based CNT memory device, enabling simultaneous implementation of both switching properties and low operation power, would pave a way toward practical memory components of next-generation portable electronic gadgets.

## Data Availability

The Figure data used to support the findings of this study are included in the article. The Figure and Table data used to support the findings of this study are included in the supplementary information file.

## Conflicts of Interest

The authors declare that they have no conflicts of interest.

## Authors' Contributions

Seyoung Oh and Seung Won Lee contributed equally to this work.

## Acknowledgments

This work was supported by the National Research Foundation of Korea (NRF) grant funded by the Korea government (MSIT; Ministry of Science and ICT) (2017R1C1B1005076).

## Supplementary Materials

Scheme of ALD process consisting of $ZrHfO_2$ (10 cycles) and Al-$ZrHfO_2$ subcycle (1 cycle) for the deposition of Al-doped $ZrHfO_2$ high-k film; X-ray diffraction peak of Al-$ZrHfO_2$ dielectric; $V_{th}$ of $Al_2O_3$ and Al-$ZrHfO_2$; $I_{DS}$ versus $V_{DS}$ for Al-$ZrHfO_2$ and $Al_2O_3$ CNT FET devices; transfer ($V_{BG}$-$I_{DS}$) curve of CNT FET device with $SiO_2$ (100 nm) dielectric; comparison of FET parameters for Al-$ZrHfO_2$ and $Al_2O_3$ CNT FET devices. *(Supplementary Materials)*

## References

[1] C. Farrera, F. Torres Andón, and N. Feliu, "Carbon nanotubes as optical sensors in biomedicine," *ACS Nano*, vol. 11, no. 11, pp. 10637–10643, 2017.

[2] H. Zhang, L. Xiang, Y. Yang et al., "High-performance carbon nanotube complementary electronics and integrated sensor systems on ultrathin plastic foil," *ACS Nano*, vol. 12, no. 3, pp. 2773–2779, 2018.

[3] J. Si, D. Zhong, H. Xu et al., "Scalable preparation of high-density semiconducting carbon nanotube arrays for high-performance field-effect transistors," *ACS Nano*, vol. 12, no. 1, pp. 627–634, 2018.

[4] C. Biswas and Y. H. Lee, "Graphene versus carbon nanotubes in electronic devices," *Advanced Functional Materials*, vol. 21, no. 20, pp. 3806–3826, 2011.

[5] W. J. Yu, S. H. Chae, S. Y. Lee, D. L. Duong, and Y. H. Lee, "Ultra-transparent, flexible single-walled carbon nanotube non-volatile memory device with an oxygen-decorated graphene electrode," *Advanced Materials*, vol. 23, no. 16, pp. 1889–1893, 2011.

[6] W. J. Yu, B. R. Kang, I. H. Lee, Y. S. Min, and Y. H. Lee, "Majority carrier type conversion with floating gates in carbon nanotube transistors," *Advanced Materials*, vol. 21, no. 47, pp. 4821–4824, 2009.

[7] M. Rinkiö, A. Johansson, G. S. Paraoanu, and P. Törmä, "High-speed memory from carbon nanotube field-effect transistors with high-$\kappa$ gate dielectric," *Nano Letters*, vol. 9, no. 2, pp. 643–647, 2009.

[8] W. Fu, Z. Xu, X. Bai, C. Gu, and E. Wang, "Intrinsic memory function of carbon nanotube-based ferroelectric field-effect transistor," *Nano Letters*, vol. 9, no. 3, pp. 921–925, 2009.

[9] W. Y. Fu, Z. Xu, L. Liu, X. D. Bai, and E. G. Wang, "Two-bit ferroelectric field-effect transistor memories assembled on individual nanotubes," *Nanotechnology*, vol. 20, no. 47, article 475305, 2009.

[10] M. Olmedo, C. Wang, K. Ryu et al., "Carbon nanotube memory by the self-assembly of silicon nanocrystals as charge storage nodes," *ACS Nano*, vol. 5, no. 10, pp. 7972–7977, 2011.

[11] J.-H. Ahn and S.-H. Kwon, "Sub-0.5 nm equivalent oxide thickness scaling for Si-doped $Zr_{1-x}Hf_xO_2$ thin film without using noble metal electrode," *ACS Applied Materials & Interfaces*, vol. 7, no. 28, pp. 15587–15592, 2015.

[12] P. K. Park and S.-W. Kang, "Enhancement of dielectric constant in $HfO_2$ thin films by the addition of $Al_2O_3$," *Applied Physics Letters*, vol. 89, no. 19, article 192905, 2006.

[13] A. Kis, G. Csányi, J. P. Salvetat et al., "Reinforcement of single-walled carbon nanotube bundles by intertube bridging," *Nature Materials*, vol. 3, no. 3, pp. 153–157, 2004.

[14] K. P. So, I. H. Lee, D. L. Duong et al., "Improving the wettability of aluminum on carbon nanotubes," *Acta Materialia*, vol. 59, no. 9, pp. 3313–3320, 2011.

[15] S. Nuriel, L. Liu, A. H. Barber, and H. D. Wagner, "Direct measurement of multiwall nanotube surface tension," *Chemical Physics Letters*, vol. 404, no. 4–6, pp. 263–266, 2005.

[16] W. H. Wang, Y. T. Lin, and C. T. Kuo, "Nanofabrication and properties of the highly oriented carbon nanocones," *Diamond and Related Materials*, vol. 14, no. 3–7, pp. 907–912, 2005.

[17] J. Müller, T. S. Böscke, U. Schröder et al., "Ferroelectricity in simple binary $ZrO_2$ and $HfO_2$," *Nano Letters*, vol. 12, no. 8, pp. 4318–4323, 2012.

[18] J. H. Sim, S. C. Song, P. D. Kirsch et al., "Effects of ALD $HfO_2$ thickness on charge trapping and mobility," *Microelectronic Engineering*, vol. 80, pp. 218–221, 2005.

[19] G. Ribes, J. Mitard, M. Denais et al., "Review on high-k dielectrics reliability issues," *IEEE Transactions on Device and Materials Reliability*, vol. 5, no. 1, pp. 5–19, 2005.

[20] H. Takeuchi, D. Ha, and T.-J. King, "Observation of bulk $HfO_2$ defects by spectroscopic ellipsometry," *Journal of Vacuum Science & Technology A: Vacuum, Surfaces, and Films*, vol. 22, no. 4, pp. 1337–1341, 2004.

[21] A. S. Foster, F. Lopez Gejo, A. L. Shluger, and R. M. Nieminen, "Vacancy and interstitial defects in hafnia," *Physical Review B*, vol. 65, no. 17, article 174117, 2002.

[22] Y. Zhang, Y. Y. Shao, X. B. Lu et al., "Defect states and charge trapping characteristics of $HfO_2$ films for high performance nonvolatile memory applications," *Applied Physics Letters*, vol. 105, no. 17, article 172902, 2014.

[23] W. Kim, A. Javey, O. Vermesh, Q. Wang, Y. Li, and H. Dai, "Hysteresis caused by water molecules in carbon nanotube field-effect transistors," *Nano Letters*, vol. 3, no. 2, pp. 193–198, 2003.